Ore genesis of the Xa Loi gold deposit, Central Vietnam: evidence from S–O–H isotopes and fluid inclusion compositions

Ngo Xuan Dac[1*], Trinh Hai Son[1], Bui The Anh[1], To Xuan Ban[2], Cao Viet Anh[3]

[1]*Vietnam Institute of Geosciences and Mineral Resources, Hanoi, Vietnam*
[2]*Hanoi University of Mining and Geology, Hanoi, Vietnam*
[3]*China University of Geosciences, Wuhan 430074, China*

ABSTRACT

The Xa Loi gold deposit, located within the Truong Son Fold Belt of central Vietnam, provides a critical case study for understanding magmatic-hydrothermal gold systems in Southeast Asia. This study integrates sulfur (δ^{34}S), oxygen-hydrogen (δ^{18}O–δD) isotopes, microthermometry, and stepwise-crushing gas-inclusion analyses to constrain the origin, evolution, and physicochemical conditions of the ore-forming fluid. Pyrite exhibits a narrow δ^{34}S range from –0.49‰ to +2.90‰, indicating a homogeneous sulfur source derived from magmatic degassing under moderately oxidizing conditions. Quartz δ^{18}O and fluid δD values plot entirely within global magmatic fields, demonstrating that the aqueous component of the hydrothermal system was sourced from a deep, evolved felsic-intermediate magma with no meteoric contribution. Fluid-inclusion gases define a H_2O–CO_2–N_2–CH_4 system characterized by $CO_2/CH_4 > 1$ and elevated N_2/Ar ratios ($\approx$400–1100), with all data plotting within the Magmatic-Evolved Magmatic fields of the CO_2/CH_4–N_2/Ar diagram. These signatures indicate a CO_2-rich, moderately oxidized magmatic fluid that underwent limited interaction with N-bearing crustal rocks during ascent. The progressive transition from SFI to Mixing and PFI inclusion populations records increasing oxidation consistent with magmatic degassing. Collectively, the S–O–H isotope systematics and gas compositions reveal that the Xa Loi gold deposit was formed by a magmatic-dominated hybrid fluid, in which sulfur, water, CO_2, and the conditions required for Au transport were supplied directly by an evolved magma and only slightly modified by crustal interaction. This genetic model highlights the role of deep magmatic processes in the formation of gold deposits along the Truong Son Fold Belt.

Keywords: Xa Loi gold deposit, S–O–H Isotopes, Fluid inclusion, Truong Son Belt.

1. Introduction

The Truong Son Fold Belt (TSFB), located in central Vietnam, represents a major Paleozoic-Mesozoic geotectonic domain within the Indochina Block. It records the complex geological evolution of the eastern Paleo-Tethys realm, including oceanic subduction, terrane accretion, arc magmatism, and multiple phases of crustal reactivation

from the Ordovician-Silurian through the Permian-Triassic (Tran et al., 2008; Tran et al., 2022). Bounded by the Song Ma Suture Zone to the north and the Tam Ky-Phuoc Son shear corridor to the south, the TSFB is subdivided into several tectonostratigraphic units that host a broad spectrum of mineral deposits formed during distinct tectonomagmatic episodes, including major granitic and volcanic events that played an essential role in crustal growth and reworking

*Corresponding author, Email: nxdac@mae.gov.vn

during the Paleozoic-Cenozoic evolution of central Vietnam (Trinh Dinh et al., 2021; Ngo et al., 2025; Nguyen et al., 2021).

This metallogenic diversity includes porphyry Cu–Au, epithermal Au–Ag, skarn, and volcanic-hosted massive sulfide (VHMS) systems. Within this regional framework, the Xa Loi-Me Xi-Dong Chat mineralized cluster in Quang Tri Province lies along the continuation of the Tam Ky-Phuoc Son shear zone, a crustal-scale transpressional fault system interpreted to have exerted strong structural control over magmatic-hydrothermal activity (Tran et al., 2008; Tran et al., 2014).

The Xa Loi gold deposit occurs as quartz–sulfide veins hosted within the Ordovician–Silurian Long Dai Formation. Geological and structural observations indicate that the mineralization is likely associated with a concealed magmatic body that provided ore-forming fluids. These fluids ascended along regional fault systems and migrated into fracture and breccia zones within the Long Dai Formation, where gold-bearing quartz veins were subsequently formed, consistent with regional patterns of intrusion-related mineralization documented elsewhere in the northern and central segments of the Truong Son Belt.

Despite this favorable geological framework, the classification and genetic interpretation of the Xa Loi deposit remain uncertain due to a lack of comprehensive geochemical, isotopic, and fluid inclusion data. As a result, several key questions remain unresolved, including: (1) the nature and source of the ore-forming fluids (magmatic, metamorphic, or mixed); (2) the physicochemical evolution of the hydrothermal system; (3) the extent of fluid-rock interaction under mid-crustal conditions; and (4) the genetic relationship between magmatic intrusions, surrounding host rocks, and gold deposition.

To address these issues, this study presents the first integrated stable isotope dataset for the Xa Loi deposit. Sulfur ($\delta^{34}S$), oxygen ($\delta^{18}O$), and hydrogen (δD) isotopic compositions from sulfides and auriferous quartz veins were analyzed to constrain the origin, composition, and evolution of the ore-forming fluids. The isotopic data are interpreted in conjunction with geological and petrographic observations to elucidate the characteristics and evolution of the hydrothermal system.

Overall, this study refines the genetic model of the Xa Loi deposit, indicating its formation from an evolved magmatic–hydrothermal system derived from a concealed magmatic source. The results contribute to a better understanding of structurally controlled, intrusion-related gold systems along the central segment of the Paleo-Tethyan margin in Southeast Asia and provide valuable insights for future regional metallogenic exploration and modeling.

2. Regional Geology

2.1. Geological setting and metallogeny

The regional tectonic framework of mainland Southeast Asia is governed by the juxtaposition of the South China and Indochina blocks along the Song Ma and Tam Ky-Phuoc Son sutures, later modified by the Cenozoic Red River shear zone. Within this architecture, the Truong Son Fold Belt (TSFB) represents a major transcurrent convergent orogenic corridor that concentrates deformation, magmatism, and hydrothermal fluid flow. The Xa Loi gold deposit is situated within the northeastern part of the TSFB, in Vinh Linh District, Quang Tri Province, central Vietnam (Fig. 1).

The area surrounding Xa Loi exposes a diverse assemblage of stratigraphic units and intrusive bodies. Quaternary sediments occupy the eastern coastal plain, whereas Neogene–Quaternary basalt occurs locally as small patches of dark-grey to light-grey massive basalt with abundant quartz–feldspar phenocrysts. Cretaceous sedimentary rocks

form a narrow strip in the southwest, consisting of conglomerate, gritstone, red silty sandstone, shale, and calcareous-siliceous breccia. Carboniferous-Permian sedimentary rocks appear as narrow belts in the central and

northwestern parts of the region, comprising silty sandstone, shale, limestone lenses, marl, weakly recrystallized dark-grey limestone, thin siliceous limestone, and coaly shale interbedded with siltstone.
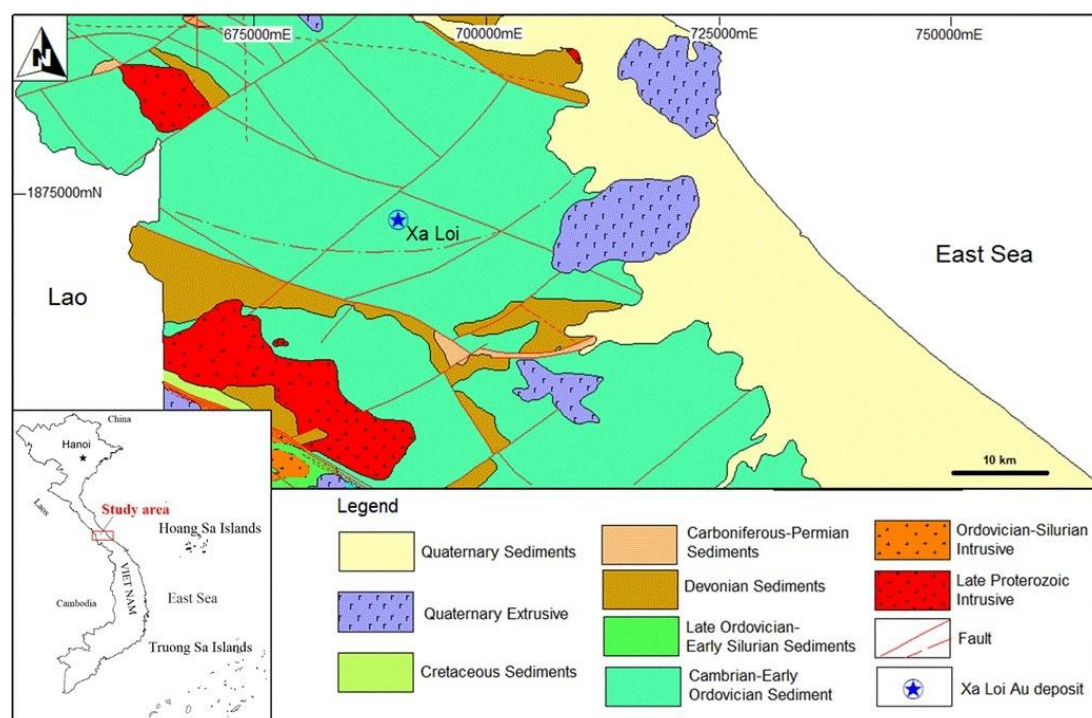

Figure 1. Regional geological map of the Xa Loi Gold Deposit, central Vietnam (after Duong et al., 1996)

Devonian strata are widely distributed in the northern and southern portions of the map area and include conglomerate, sandstone, siltstone, thin shale beds, quartzitic sandstone, and grey to dark-grey limestone intercalated with calcareous shale, cherty lenses, and weakly dolomitized limestone. The Late Ordovician-Early Silurian sedimentary sequence forms the most extensive unit in the region. It consists of thin-bedded banded shale, micaceous sandstone, chert, tuffaceous sandstone and conglomerate, and sandstone interlayered with intermediate to felsic volcanic rocks, together with quartzitic sandstone and calcareous shale. Cambrian–Early Ordovician rocks crop out as a small arcuate belt in the southwest and comprise quartz-feldspar schist, quartz-mica schist, and

quartzitic sandstone.

Two intrusive suites cut across this stratigraphic framework. Late Paleozoic intrusive bodies occur as equant and elongated masses in the northwest and southwest, including gabbro, gabbrodiorite, quartz diorite, biotite-hornblende granodiorite, biotite-hornblende granite, granite, and aplite veins. The Ordovician-Silurian intrusive rocks form an arcuate zone crosscutting Cambrian-Ordovician sediments and consist of quartz diorite, biotite granodiorite, and biotite granite. NE dissects the entire region-SW and NW-SE trending faults, which exert strong control on lithological distribution and provide important conduits for hydrothermal fluid migration and localization of gold mineralization at Xa Loi.

2.2. Geology of the Xa Loi Deposit

The Xa Loi gold deposit is hosted within the Ordovician-Early Silurian Long Dai Formation, which is mainly composed of phyllitic siltstone, fine to medium-grained quartz sandstone, feldspathic sandstone, and subordinate calcareous phyllite (Fig. 2). These rocks are typically interbedded and display rhythmic layering.

Within this sedimentary sequence, several fault systems are developed, among which the Xa Loi-Dong Chat reverse fault is the dominant structural feature. This fault trends northeast-southwest (NE–SW) and dips steeply to the south, serving as the principal structural control for hydrothermal fluid migration and gold mineralization. Secondary faults trending northwest-southeast (NW-SE) and north-south (N-S) act as subsidiary conduits, forming favorable intersection geometries for ore concentration.
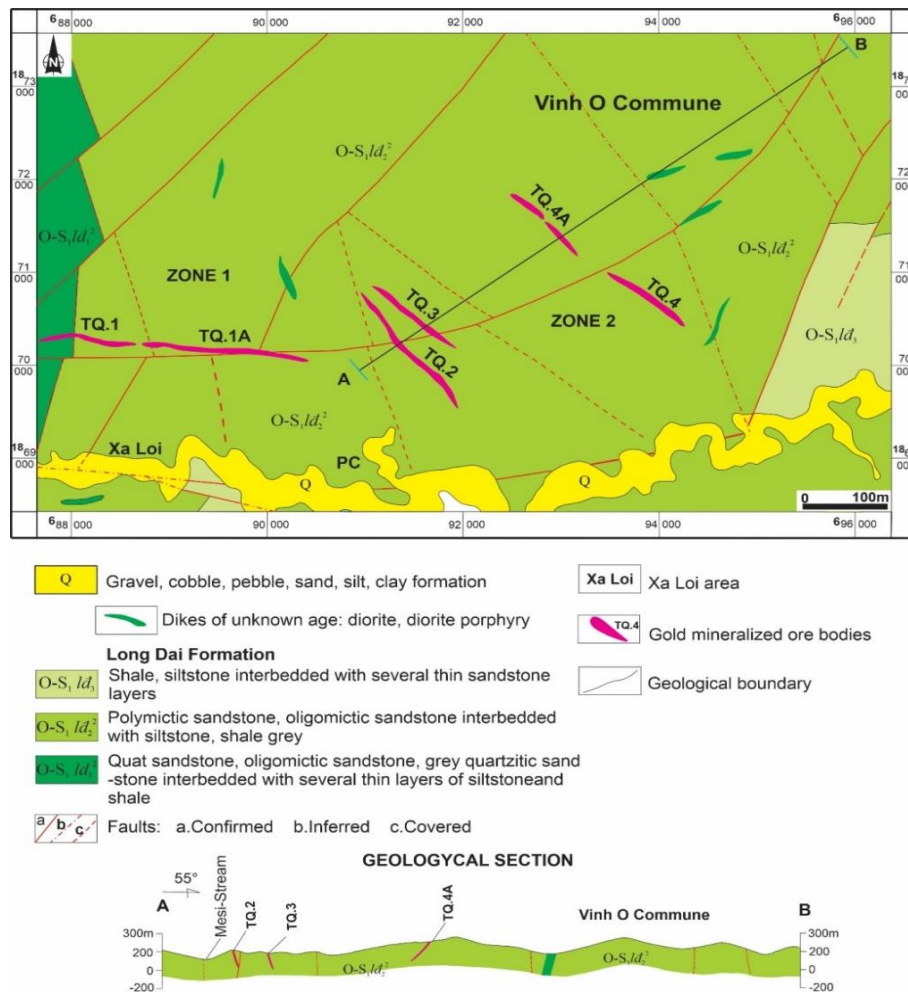

Figure 2. Geological map of the Xa Loi Gold deposit

Mafic intrusive rocks are common in the area and include fine-grained greenish doleritic dikes and porphyritic mafic intrusions. These bodies cut through the sedimentary strata and have induced extensive hydrothermal alteration. Petrographically, the porphyritic dolerite contains about 40% ferromagnesian minerals (including olivine,

28

pyroxene, biotite, and hornblende) and 60% plagioclase feldspar. Hydrothermal alteration has resulted in partial replacement of primary minerals by chlorite, epidote, and sericite (Le et al., 2025a,b).

Both the mafic dikes and the surrounding metasedimentary rocks are crosscut by quartz-sulfide veins, which represent the main ore-bearing structures. These veins commonly contain pyrite, arsenopyrite, pyrrhotite, sphalerite, galena, and chalcopyrite, and are associated with wall-rock alteration zones composed of sericite, chlorite, epidote, quartz, and limonite.

In addition, diorite porphyry dikes containing plagioclase phenocrysts and a fine-grained biotite-hornblende groundmass occur along major fault zones. These dikes are strongly altered to a propylitic assemblage consisting of chlorite, epidote, albite, quartz, and sericite. Gold has been identified along the altered margins of these intrusions, suggesting that the magmatic source contributed either metals or thermal energy to drive convective hydrothermal circulation.

In summary, the geological characteristics of the Xa Loi deposit, including the hydrothermally altered lithological assemblage and its close spatial relationship with intrusive rocks, are typical of a structurally controlled hydrothermal gold system. Fault-fault intersections and favorable host lithologies provided ideal physical and chemical traps for gold precipitation from magmatic-hydrothermal fluids that played a dominant role in ore formation (Le et al., 2025a,b).

2.3. Mineralization Characteristics of the Xa Loi Deposit

2.3.1. Ore Body Distribution and Morphology

Structures firmly control gold mineralization at the Xa Loi deposit and occur in seven distinct ore bodies, designated as TQ.1, TQ.1A, TQ.2, TQ.3, TQ.4, and TQ.4A

(Fig. 2). These ore bodies trend northeast-southwest (NE-SW) to nearly north-south (N-S), distributed along fault systems within the mining area. The ore bodies are hosted in the Ordovician-Silurian Long Dai Formation (O–S_1ld^2), which mainly consists of phyllite, quartz sandstone, and siltstone.

TQ.1 is the largest ore body in the deposit, extending approximately 800–1000 m along strike, with an actual thickness of 2–4 m (average ~ 3.3 m), and traceable to depths greater than 40 m. This ore body occurs in the sedimentary rocks of the Long Dai Formation, developed along fracture and breccia zones within the mining area. Beneath TQ.1, at shallow depth, the TQ.1A ore body has been encountered, exhibiting a corrected thickness of 0.8–1.2 m (Fig. 2).

Ore bodies TQ.2, TQ.3, TQ.4, and TQ.4A are distributed subparallel to TQ.1 in the central part of the Xa Loi deposit (Fig. 2). They occur along the mine-scale fault systems. They are hosted in sedimentary rocks, with strike lengths of several hundred meters and variable thicknesses ranging from less than 1 m to several meters. However, their continuity at depth remains uncertain due to limited drilling data.

Field observations indicate that gold mainly occurs in quartz–sulfide veins cutting across the Long Dai Formation. At the ore-body scale, quartz–gold zones are well developed within strongly altered wall rocks characterized by silicification and sericitization, forming subparallel or gently convergent vein systems (Fig. 3A, B). The quartz-gold veins range from a few centimeters to about 2 m in thickness, occurring along fracture and breccia zones, and commonly cutting across bedding planes of the Long Dai sedimentary rocks. In some localities, the veins develop into small stockwork-type vein networks (Fig. 3C). Underground workings reveal thin, discrete veins with similar orientations and clear

crosscutting relationships, emphasizing the role of fault systems as the main conduits for

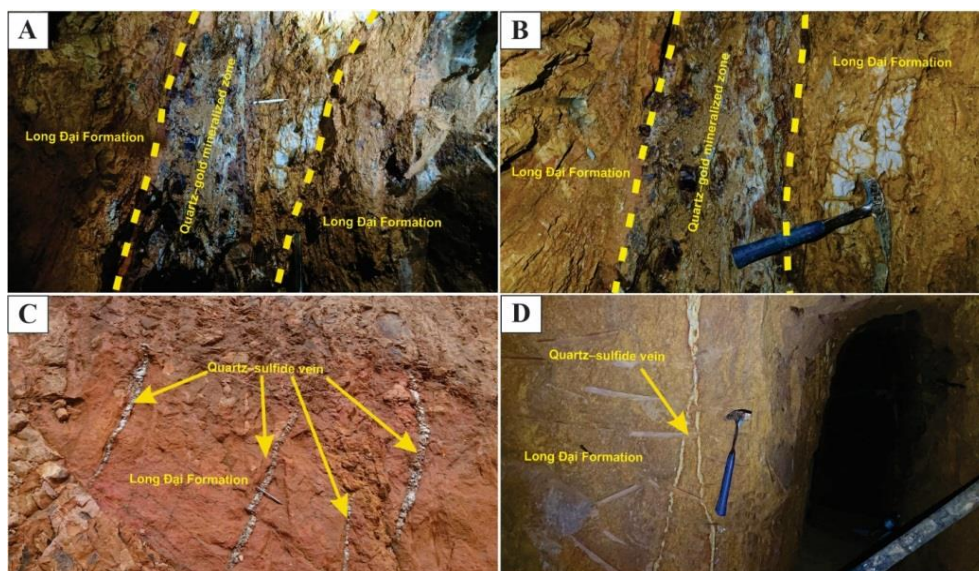the migration of magmatic–hydrothermal fluids and gold deposition (Fig. 3D).

Figure 3. Field photographs (A-D) showing quartz-sulfide gold ore bodies and quartz-sulfide gold microveins hosted within the Long Dai Formation

2.3.2. Mineralogy, Textural Characteristics, and Hydrothermal Alteration

Hand specimens of quartz–sulfide veins from the Xa Loi gold deposit clearly exhibit a quartz–pyrite–gold mineral assemblage, indicating co-crystallization during a single ore-forming stage. Pyrite occurs as fine- to medium-grained crystals disseminated within the quartz matrix, and is locally concentrated into pyrite-rich pockets (Fig. 4A, B).

From these samples, thin sections and polished slabs were prepared for petrographic and ore-mineralogical analyses to determine the paragenetic sequence of ore minerals and identify hydrothermal alteration styles associated with gold mineralization (Fig. 4C, D).

The ore mineral assemblage is dominated by pyrite, accompanied by native gold and minor chalcopyrite and arsenopyrite. Pyrite appears as euhedral to subhedral crystals (0.1–1.0 mm) and is locally altered to limonite. Native gold occurs as fine inclusions within

pyrite, and remains preserved even when pyrite is fully oxidized (Fig. 5A, B), demonstrating synchronous precipitation of gold and pyrite.

Chalcopyrite is less abundant and typically occurs as micron-scale inclusions within larger pyrite grains, indicating contemporaneous crystallization with pyrite (Fig. 5C, D, E). Arsenopyrite is rare, present as anhedral grains dispersed within the quartz matrix alongside pyrite (Fig. 5F).

Thin-section observations of gold-rich samples reveal intense sericitization closely associated with the quartz–pyrite–gold assemblage. Platy sericite commonly rims pyrite crystals, forms narrow bands or aggregates along pyrite margins, and appears as thin veinlets cutting the quartz matrix. Local sericite clusters are also concentrated at quartz–pyrite contacts. This alteration pattern confirms that sericitization is spatially linked to gold mineralization within the quartz-sulfide vein system (Fig. 6A–D).
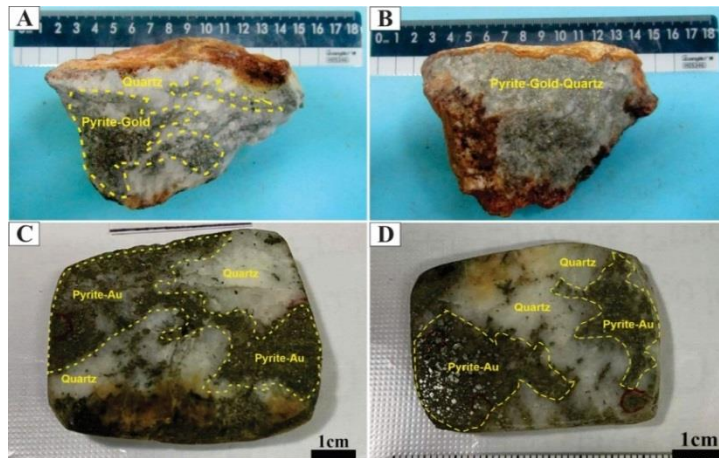
Figure 4. Hand specimens (A-D) of quartz-sulfide gold ore selected for sulfur, oxygen-hydrogen isotope, and fluid-inclusion analyses
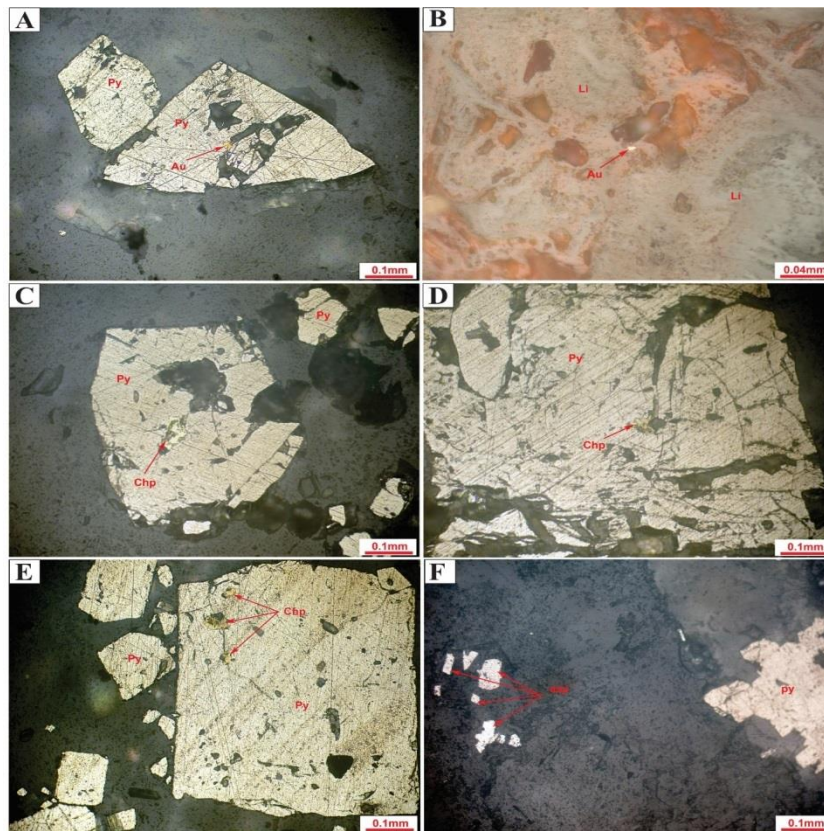
Figure 5. Reflected-light photomicrographs of auriferous sulfide ore samples. (A-B) Native gold (Au) occurs as fine grains disseminated within pyrite (Py) and limonite (Li), the latter representing complete alteration of pyrite. (C-E) Chalcopyrite (Chp) appears as fine inclusions distributed along fractures and grain boundaries of pyrite (Py). (F) Arsenopyrite (Asp) occurs as anhedral grains disseminated and intergrown with pyrite (Py)

Figure 6. A-D are photomicrographs taken under plane-polarized light (one nicol) and cross-polarized light (two nicols), showing sericitic hydrothermal alteration closely associated with gold mineralization.
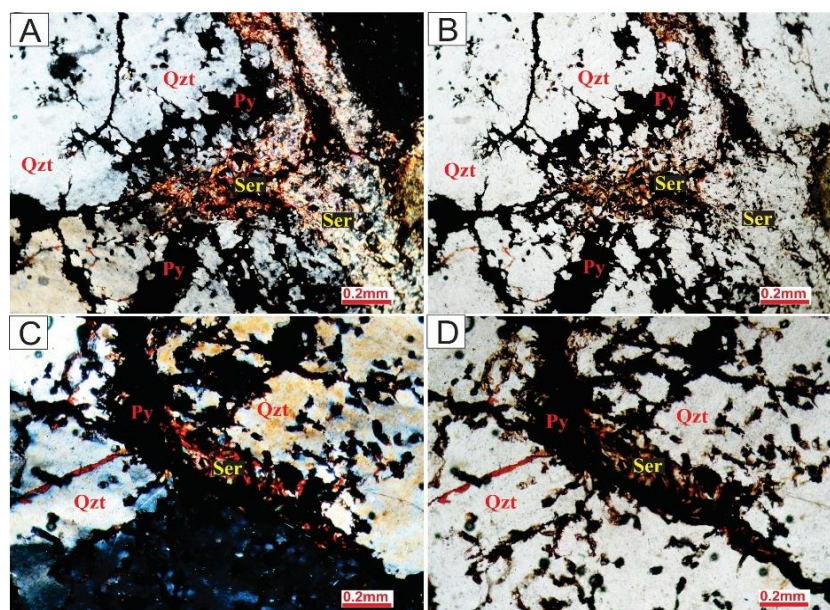Abbreviate: Qzt: Quartz, Py: Pyrite, Ser: Sericite

3. Sample and Analytical Methods

3.1. Sample

All sulfide samples selected for sulfur isotope analysis were collected from gold-bearing quartz-sulfide veins representing the main hydrothermal mineralization stage of the Xa Loi deposit.

These veins are typically dominated by pyrite, with subordinate arsenopyrite and chalcopyrite, and commonly contain visible native gold. Sulfide minerals were handpicked from these veins under a binocular microscope to ensure purity and to avoid contamination by gangue minerals. The quartz samples used for oxygen-hydrogen isotope and fluid-inclusion analyses were collected from the same quartz-sulfide veins that host gold mineralization (Fig. 3A–B).

3.2. Analytical Methods

3.2.1. Sulfur Isotope Analysis

Sulfur isotope analyses were conducted at Guangzhou Tuoyan Testing Technology Co., Ltd. using a Thermo Fisher MAT 253 Plus mass spectrometer coupled with a Flash EA elemental analyzer and a Conflo IV interface

Samples (<100 μg S) were sealed in tin capsules and combusted at 960–1020°C, with oxygen supplied to ensure complete oxidation. Combustion gases were carried by helium through a WO_3–Cu redox reactor, converting all sulfur species to SO_2, which was then separated by a dedicated sulfur chromatographic column before entering the mass spectrometer.

International standards used included IAEA-SO-5, IAEA-SO-6, NBS 127, IAEA-S3, GBW04414, and GBW04415. Analytical precision for $\delta^{34}S$ was better than ±0.2‰, and reference materials yielded values consistent with certified standards. Sulfur content was calculated from the peak area.

3.2.2. Oxygen Isotope Analysis

Oxygen isotope analyses of quartz were

carried out at Guangzhou Tuoyan Analytical Technology Co., Ltd. The samples were first ground to 200 mesh. Approximately 6 mg of pure quartz or silicate mineral powders (with equivalent oxygen content) were weighed and baked at 105°C for 12 hours to remove moisture.

Oxygen was extracted using the BrF₅ method (Clayton et al., 1963). In this procedure, the samples were reacted with BrF₅ under vacuum at 580°C to release O₂ gas. The released gas was purified using 5 Å molecular sieve traps and then introduced into a Thermo Fisher 253 Plus isotope ratio mass spectrometer for $\delta^{18}O$ measurement. The results are reported relative to the V-SMOW standard, with an external analytical precision better than ±0.2‰, and the measured values of the reference standards were consistent with their recommended values.

To estimate the $\delta^{18}O$ composition of hydrothermal fluids, values were calculated using the quartz-water oxygen isotope fractionation equation proposed by Clayton et al. (1972):

$$1000\ln\alpha_{quartz-water} = \frac{3.38\times10^6}{T^2} - 3.40$$

Where T is the temperature in Kelvin, and α is the quartz–water isotope fractionation factor, calculated as:

$$\alpha = \frac{(\delta^{18}O_{quartz}+1000)}{(\delta^{18}O_{water}+1000)}$$

3.2.3. Hydrogen Isotope Analysis

Hydrogen isotope analyses of fluid inclusions were carried out at Guangzhou Tuoyan Analytical Technology Co., Ltd., China. Approximately 10–20mg of quartz single-mineral grains (40–60 mesh) were weighed and placed in a tin capsule, then heated in a 90°C oven for 12 hours to remove adsorbed surface water. After drying, the tin-wrapped samples were introduced into a high-

temperature pyrolysis furnace (Flash EA, Thermo) packed with glassy carbon and maintained at 1420°C via an autosampler. Water released from fluid inclusions reacted instantaneously with carbon to produce H₂ and CO. These gases were carried by high-purity helium (5N) through a chromatographic column and introduced into a Thermo Fisher 253 Plus isotope ratio mass spectrometer for the determination of the hydrogen isotopic ratio (δD). The international reference materials used include biotite USGS57 (δD_{V-SMOW} = −91‰), muscovite USGS58 (δD_{V-SMOW} = −28‰), and polyethylene IAEA-CH-7 (δD_{V-SMOW} = −100.3‰). The analytical precision is better than ±1‰, and the measured values of the reference materials were consistent with their recommended values.

3.2.4. QMS composition analysis

Gases released from fluid inclusions in two quartz vein samples were analyzed using a Hiden HAL 1051–9 PIC® quadrupole mass spectrometer (QMS) with ion-counting detection (MASsoft control). The instrument covers m/z 1–50, allowing identification of major magmatic–hydrothermal gases. Analyses were conducted at the Fluid Inclusion and Noble Gas Laboratory, China University of Geosciences (Wuhan).

Stepwise-crushing method Gas extraction followed the stepwise-crushing technique modified after Qiu & Wijbrans (2006), Qiu & Jiang (2007), and Qiu et al. (2011). The system consists of a mechanical crusher connected to a Pfeiffer HiCube80 Eco™ turbo-pumping station. Quartz grains (380–830 μm) were purified, ultrasonically cleaned, and ~150 mg was loaded into a 316L stainless-steel crushing tube with a 3Cr13 (S42030) steel pestle. The pestle (214 g) was

magnetically lifted and released 3–5 cm per drop, applying low-force incremental crushing to avoid gas surges (see Andrawes & Gibson, 1979; Matsumoto et al., 2001).

Analytical procedure All measurements were performed at room temperature under high vacuum (4.0×10^{-8} mbar). A procedural blank was recorded before each run. Gas released at each crushing step was expanded into the QMS and analyzed in static mode. Histogram scans (m/z 1–65) were collected with 70 eV ionization energy, and base peaks were selected to avoid overlapping fragments. The vacuum line and crusher were baked at 150°C for ~20 h before analysis and turbo-pumped between steps. Post-run procedures followed Xiao et al. (2019).

4. Results

4.1. Sulfur Isotope

Five sulfide samples (pyrite) from the Xa Loi gold deposit were analyzed for $\delta^{34}S_{V-CDT}$ values, ranging from –0.49‰ to +2.90‰. Most values cluster between +0.90‰ and +1.93‰, with only one sample exhibiting a slightly negative value (–0.49‰). The average $\delta^{34}S$ value is approximately +1.57‰, reflecting a narrow and moderately positive range. The detailed analytical results are presented in Table 1.

Table 1. $\delta^{34}S$ Values of pyrite from the Xa Loi Gold Deposit

No	Sample	Mineral	$\delta^{34}S_{V-CDT}$(‰)
1	Xl 01	Pyrite	0.90
2	Xl 02	Pyrite	1.60
3	Xl 03	Pyrite	1.93
4	Xl 04	Pyrite	2.90
5	Xl 05	Pyrite	-0.49

4.2. Oxygen Isotope

Oxygen isotope analyses of five quartz samples from the Xa Loi gold deposit yield $\delta^{18}O_{V-SMOW}$ values ranging from 12.95‰ to 13.34‰. Assuming isotopic equilibrium between quartz and hydrothermal fluids at temperatures of 250–350°C, the calculated $\delta^{18}O_{H_2O}$ values vary from 4.00‰ to 8.04‰. The detailed analytical results are presented in Table 2.

Table 2. $\delta^{18}O$ Values of Quartz from the Xa Loi Gold deposit

No	Sample	Mineral	$\delta^{18}O_{V-SMOW}$(‰)	$\delta^{18}O_{H_2O}$ at 250°C	$\delta^{18}O_{H_2O}$ at 300°C	$\delta^{18}O_{H_2O}$ at 325°C	$\delta^{18}O_{H_2O}$ at 350°C
1	Xl 01	Quartz	13.22	4.27	6.33	7.17	7.92
2	Xl 02	Quartz	13.34	4.39	6.45	7.29	8.04
3	Xl 03	Quartz	13.31	4.36	6.42	7.26	8.01
4	Xl 04	Quartz	13.31	4.36	6.42	7.26	8.01
5	Xl 05	Quartz	12.95	4.00	6.06	6.90	7.65

4.3. Hydrogen Isotope

Hydrogen isotope compositions (δD_{V-SMOW}) The fluid inclusion counts in quartz samples were determined for five representative samples. The δD values range from –70.5‰ to –63.5‰, showing a relatively narrow variation among the quartz-hosted fluid inclusions. The detailed results are summarized in Table 3.

Table 3. δD_{V-SMOW} (‰) Values of Quartz from the Xa Loi Gold deposit

No	Sample	Mineral	δD_{V-SMOW} (‰)
1	Xl 01	Quartz	-70.5
2	Xl 02	Quartz	-65.7
3	Xl 03	Quartz	-65.5
4	Xl 04	Quartz	-63.5
5	Xl 05	Quartz	-69.7

4.4. QMS gas composition analysis

The complete dataset is summarized in Table A.1 and illustrated in Figs. 9–10.

Sample XL01, the SFI stage (steps 1–26) is characterized by CO_2/CH_4 = 1.01–2.40 (average 1.99), indicating a weakly oxidizing environment, still retaining some CH_4 but clearly not reducing. CO_2 (12.82–23.63 mol%) and N_2 (63.70–80.52 mol%) remain relatively stable, while CH_4 (5.61–10.36 mol%) gradually decreases, reflecting partial degassing. During the Mixing stage (steps 27–51), the CO_2/CH_4 ratio increases to 2.31–2.89 (average 2.59), marking a clear rise in oxidizing conditions, accompanied by a significant increase in N_2 (79.65–90.00 mol%) and a decrease in CH_4 (2.69–5.30 mol%). This transitional stage corresponds to progressive chemical and redox changes in the fluid. In the PFI stage (steps 52–74), CO_2/CH_4 increases further to 2.58–4.12 (average 3.51), while N_2 reaches 89.60–97.43 mol% and CH_4 declines to 0.46–2.55 mol%. CO_2 decreases to 1.77–7.64 mol%.

In Sample XL02, the same evolutionary trend is observed, but with overall higher oxidation levels. In the SFI stage (steps 1–24), CO_2/CH_4 = 1.81–2.58 (average 2.22), reflecting a weakly to moderately oxidized environment, with CO_2 (18.01–25.43 mol%) and CH_4 (6.98–11.33 mol%), and N_2 = 51.53–74.16 mol%. During the Mixing stage (steps 25–44), CO_2/CH_4 increases to 2.96–4.14 (average 3.59), and N_2 rises to 68.57–77.94 mol%, indicating a further strengthening of oxidizing conditions similar to XL01, but more pronounced. In the PFI stage (steps 45–62), CO_2/CH_4 reaches the highest values (4.12–5.90; average 5.10), with N_2 = 70.13–94.43 mol% and CH_4 reduced to 0.75–6.43 mol%.

5. Discussions

5.1. Sulfur Isotopic Values

Five pyrite samples from the Xa Loi gold deposit yield $\delta^{34}S$ values between –0.49‰ and +2.90‰ (Table 1), representing a narrow interval centered near 0‰. This restricted range indicates a relatively homogeneous sulfur source and is typical of reduced sulfur (H_2S, S^{2-}) derived from magmatic degassing under moderately oxidizing magmatic-hydrothermal conditions (Ohmoto & Rye, 1979; Seal, 2006). Compared with global $\delta^{34}S$ fields for major ore deposit types (Fig. 7), the Xa Loi pyrite values fall entirely within the range of deep-sourced magmatic-hydrothermal systems and are clearly distinct from both the highly negative $\delta^{34}S$ values (< –10‰) characteristic of biogenic sulfate reduction in sedimentary environments, and the highly positive $\delta^{34}S$ signatures (+10‰ to +35‰) of marine sulfate (Claypool et al., 1980). The narrow isotopic interval among all five samples suggests that sulfur was supplied from a single, internally consistent magmatic reservoir, with negligible contribution from sedimentary, evaporitic, or organic-derived sulfur. Importantly, no isotopically light sulfur is present, contrary to what would be expected if sedimentary sulfate reduction or organic matter decomposition had significantly contributed to the hydrothermal system. In contrast, the Me Xi deposit in the duplicate structural corridor records lighter $\delta^{34}S$ values (–4.6‰ to –0.2‰) and even lower values in brecciated zones (down to –8.6‰; Le et al., 2025b), demonstrating partial involvement of sedimentary sulfur there but not at Xa Loi.
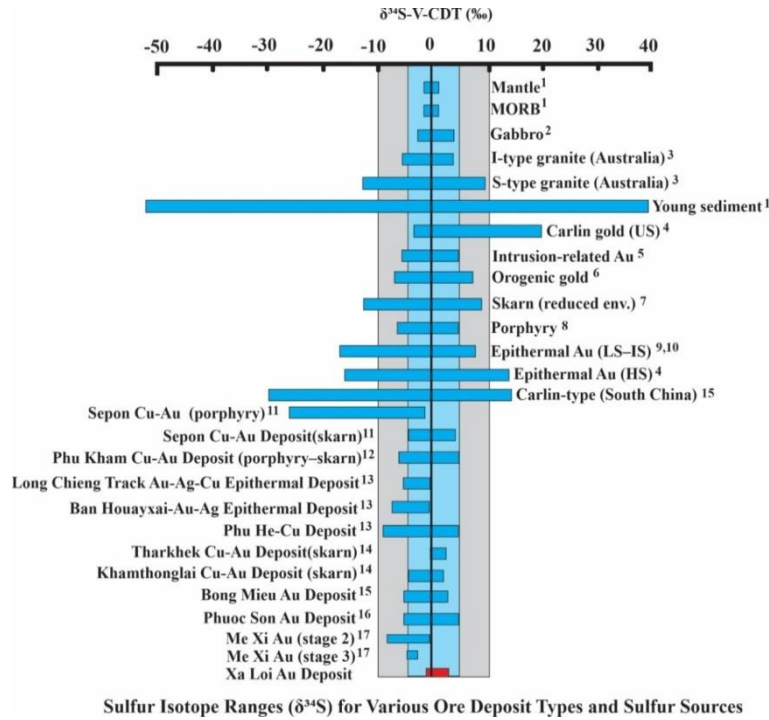
Figure 7. Comparison of sulfur isotope (δ³⁴S) values from the Xa Loi gold deposit with those from various gold and Cu–Au deposits, as well as with sulfur isotope compositions from selected geological sources (mantle, MORB, granite, gabbro). References: 1. Rollinson (1993); 2. Sasaki and Ishihara (1979); 3. Coleman (1977); 4 Hofstra and Cline (2000); 5.Thompson and Newberry (2000), 6. Hodkiewicz et al. (2009); 7. Zaw et al. (2007); 8. Cooke and Simmons (2000); 9. Christie et al. (2007); 10. Camprubi and Albinson (2007), 11. Cromie (2010), 12.Backhouse (2004), 13. Manaka (2008), 14. Hotson (2009), 15. Ngo (2024); 16. Manaka (2014). 17. Le et al. (2025b)

5.2. Oxygen and Hydrogen Isotopic Values

Five quartz samples from the Xa Loi gold deposit display tightly clustered $\delta^{18}O_{Qtz}$ values of 12.95‰ to 13.34‰ (average ≈13.23‰ V-SMOW; Table 2), indicating that the hydrothermal system was well buffered and experienced minor isotopic modification from external fluids. Homogenization temperatures of fluid inclusions in the same quartz samples range between 250 and 350°C (Ngo et al., 2025). Using the quartz-water fractionation equation of Clayton et al. (1972), the calculated $\delta^{18}O_{H_2O}$ values span 4.00–4.39‰ at 250°C, 6.06–6.45‰ at 300°C, 6.90–7.29‰ at 325°C, and 7.65–8.04‰ at 350°C (Table 2). Across the overall temperature range, $\delta^{18}O_{H_2O}$ varies from ~4.0‰ to ~8.0‰, and values

calculated above 300°C fall entirely within the field of evolved magmatic waters (≈5–10‰; Taylor, 1979; Ohmoto & Rye, 1979) (Fig. 8). The lowest value (~4‰ at 250°C) approaches the lower limit of metamorphic fluids but is best interpreted as reflecting late-stage cooling of a dominantly magmatic fluid. Analytical reliability is confirmed by the quartz standard GBW04421 (10.95‰ vs. the certified value of 10.92‰).

The metamorphic water box, kaolinite weathering line, and meteoric water line are from Giggenbach (1992) and Hoefs (2009). The δD values of liquid-vapor inclusions range from –70.5‰ to –63.5‰ (average –66.3‰; Table 3), which lie squarely within the characteristic magmatic field (≈ –40 to –80‰; Sheppard, 1986) and are distinctly

heavier than typical meteoric water ($\approx$ –80 to –120‰; Craig, 1961). The combined δD–$\delta^{18}O$ data therefore indicate that the ore-forming

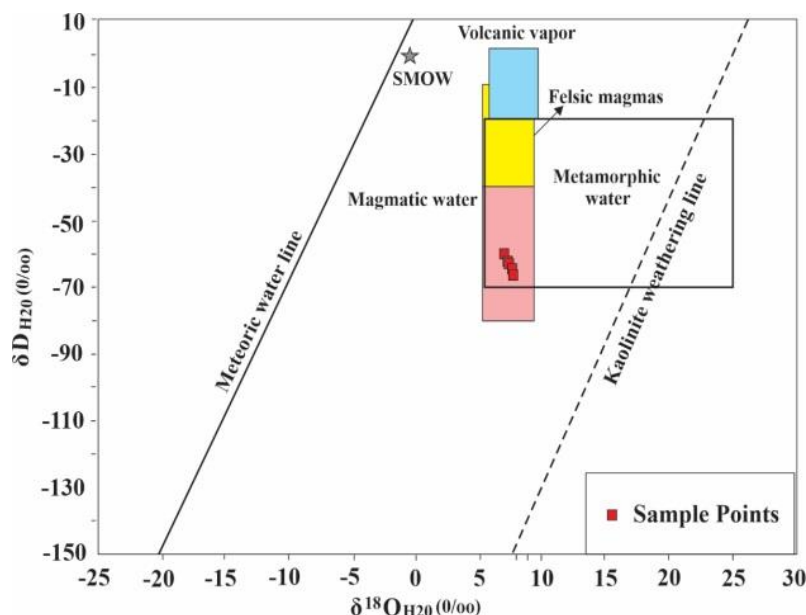fluid was derived from a deep, evolved magmatic reservoir with no evidence for meteoric water input.

Figure 8. $\delta^{18}O$ versus δD isotope compositions of the Xa Loi mineralizing fluids. Fields of volcanic vapor, felsic magma, and magmatic water are from Hedenquist & Lowenstern (1994)

5.3. Gas Composition and Fluid Evolution

Stepwise-crushing analyses of fluid inclusions from samples XL01 and XL02 reveal an H_2O–CO_2–N_2–CH_4 system characteristic of deep hydrothermal fluids. The systematic increase in CO_2/CH_4 ratios across SFI $\rightarrow$ Mixing $\rightarrow$ PFI stages ($\approx$1.8–2.6 $\rightarrow$ 2.3–4.1 $\rightarrow$ 2.6–5.9) indicates progressive oxidation during fluid evolution, consistent with ascent and magmatic degassing processes (Fig. 9A, 10A). Correspondingly, variations in gas concentrations define three inclusion populations representing distinct trapping stages (Fig. 9B, 10B).

On the CO_2/CH_4–N_2/Ar diagrams (Norman & Moore, 1999), all inclusion groups fall within or near the Magmatic and Evolved Magmatic fields (Fig. 9C–D; Fig. 10C–D), confirming that the ore fluid is dominantly magmatic rather than metamorphic-organic. Notably, SFI populations already lie beyond the Organic fluid field (CO_2/CH_4 > 1;

N_2/Ar >100), and later inclusion stages trend toward higher CO_2/CH_4 ratios, reflecting oxidation during fluid ascent.

The very high N_2/Ar ratios ($\approx$400–1100) indicate that the fluid interacted with nitrogen-bearing crustal rocks. This N_2 input likely originated from organic-rich or NH_4^+-bearing lithologies (Potter et al., 2004; Watenphul et al., 2009). However, this crustal nitrogen addition did not modify the magmatic-hydrothermal nature of the fluid, as long as the CO_2/CH_4 ratio remained >1 (Norman & Moore, 1999). The overlapping PFI compositions of samples XL01 and XL02 further suggest that they experienced similar fluid–rock interaction pathways.

Overall, the gas-inclusion data demonstrate that Xa Loi ores formed from an evolved, moderately oxidized magmatic fluid, modified during ascent by interaction with crustal rocks, consistent with fluid evolution in magmatic-orogenic gold systems.

Figure 9. Stepwise-crushing gas inclusion results for sample XL01. (A) CO_2/CH_4 ratios showing three inclusion populations. (B) Relative abundances of major gases (CH_4, H_2O, N_2, Ar, CO_2) released during crushing. (C) CO_2/CH_4 vs. N_2/Ar plot (after Norman & Moore, 1999). (D) Simplified CO_2/CH_4–N_2/Ar distribution highlighting the progressive fluid evolution

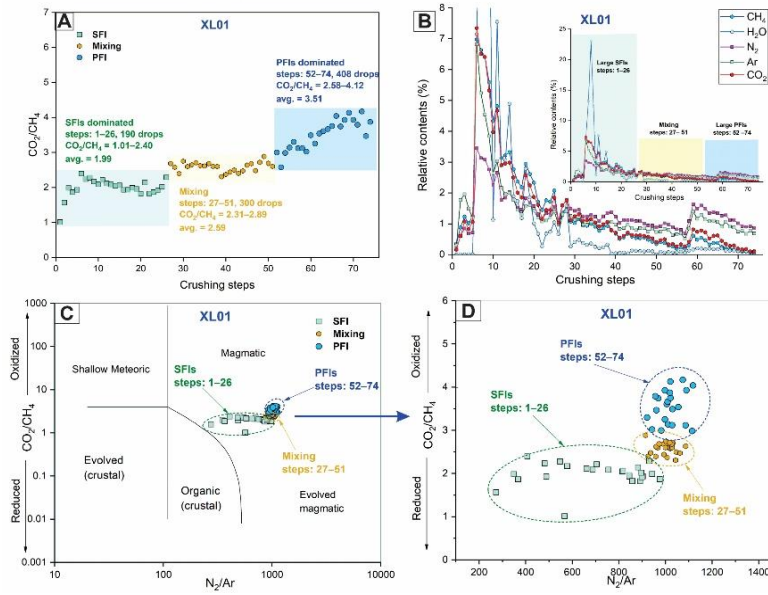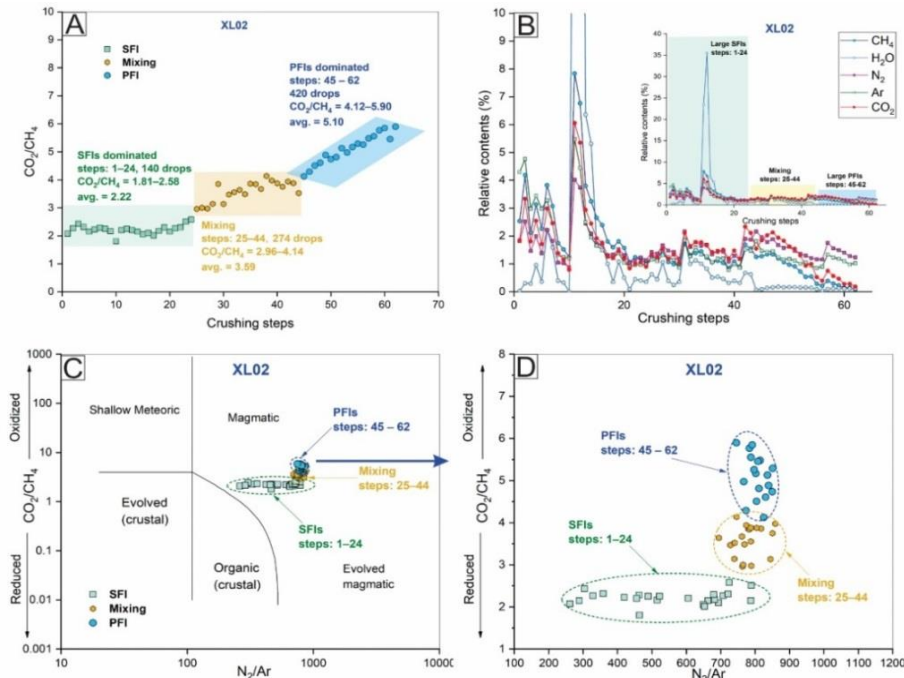*Figure 10*. Stepwise-crushing gas inclusion results for sample XL02. (A) CO_2/CH_4 ratios showing three inclusion populations. (B) Relative abundances of major gases (CH_4, H_2O, N_2, Ar, CO_2) released during crushing. (C) CO_2/CH_4 vs. N_2/Ar plot (after Norman & Moore, 1999). (D) Simplified CO_2/CH_4–N_2/Ar distribution highlighting the progressive fluid evolution

5.4. Integrated S–O–H Isotopes and Fluid-Inclusion Gases: Genetic Implications

Sulfur isotope compositions at Xa Loi ($\delta^{34}S \approx$ –3.9‰ to +0.3‰) define a narrow, near-zero range consistent with sulfur derived from a single magmatic reservoir in equilibrium with H_2S–SO_2 under intermediate fO_2 conditions (Ohmoto & Rye, 1979; Seal, 2006). The absence of isotopically light or heavy sulfur excludes contributions from sedimentary sulfate, organic matter, or evaporites, in contrast to deposits like Me Xi, where sedimentary sulfur plays a role.

Oxygen–hydrogen isotopes independently reinforce this magmatic origin: calculated $\delta^{18}O_{H_2O}$ and measured δD values fall squarely within magmatic fluid fields and are clearly distinct from meteoric or metamorphic water signatures (Taylor, 1979; Sheppard, 1986). These isotopic systematics indicate that the Xa Loi ore fluid remained well-buffered and did not mix with shallow fluids during ascent.

The gas-inclusion results provide further constraints by confirming moderate oxidation and showing that magmatic fluids interacted with crustal wall rocks, enriching N_2 without changing the isotopic character of sulfur or water. This consistency across S–O–H isotope systems and gas compositions demonstrates that both the aqueous and sulfur components of the fluid share a common deep-seated magmatic source. Collectively, these data define a magmatic-dominated hydrothermal system in which both sulfur and water were sourced from an evolved felsic-intermediate magma, the fluid evolved under moderately oxidizing conditions near the FMQ buffer, and interaction with crustal wall rocks was limited sufficient only to introduce additional N_2 without modifying the magmatic isotopic signatures. This fluid configuration is fully consistent with global magmatic-orogenic gold models (Goldfarb & Groves, 2015; Goldfarb, 2023), in which CO_2–H_2O-rich magmatic fluids ascend along deep crustal faults, undergo progressive oxidation, and ultimately precipitate gold under mesozonal conditions within tectonic belts such as the Truong Son Fold.

6. Conclusions

Integrated S–O–H isotope data, fluid-inclusion gases, and microthermometry collectively indicate that the Xa Loi gold deposit formed from a deep, CO_2-rich, moderately oxidized magmatic-hydrothermal fluid. The tight $\delta^{34}S$ range near 0‰, together with $\delta^{18}O_{H_2O}$ ($\approx$4–8‰) and δD ($\approx$–70‰), confirms a homogeneous magmatic source with no sedimentary, organic, or meteoric input. Stepwise-crushing results ($CO_2/CH_4 > 1$; $N_2/Ar \approx 400$–1100) plot within magmatic-evolved magmatic fields, reflecting magmatic redox conditions and minor interaction with N-bearing crustal rocks. The SFI → Mixing → PFI sequence records progressive oxidation during fluid ascent. Overall, Xa Loi represents a structurally focused magmatic-hydrothermal gold system, where sulfur, water, CO_2, and gold-transport conditions were primarily magma-derived and only slightly modified during crustal passage within the Truong Son Fold Belt.

Acknowledgements

References

Andrawes F.F., Gibson E.K. Jr., 1979. Release and analysis of gases from geological samples. American Mineralogist, 64, 453–463.

Backhouse W.V., 2004, Geological setting, alteration and nature of mineralisation at Phu Kham copper-gold deposit, Lao PDR: Unpub. (Hons) thesis, University of Tasmania.

Camprubí A., Albinson T., 2007. Epithermal deposits in México Update of current knowledge, and an empirical reclassification.
https://doi.org/10.1130/2007.2422(14).

Chiodini G., et al., 2004. Magmatic degassing and temperature-pressure conditions beneath geothermal fields. Earth and Planetary Science Letters, 222, 469–484.

Christie A.B., Simpson M.P., Brathwaite R.L., Mauk J.L., Simmons S.F., 2007. Epithermal Au-Ag and related deposits of the Hauraki goldfield, Coromandel volcanic zone, New Zealand: Economic Geology, 102, 785–816.

Claypool G.E., Holser W.T., Kaplan I.R., Sakai H., Zak I., 1980. The age curves of sulfur and oxygen isotopes in marine sulfate and their mutual interpretation. Chemical Geology, 28, 199–260.

Clayton R.N., Mayeda T.K., 1963. The use of bromine pentafluoride in the extraction of oxygen from oxides and silicates for isotopic analysis. Geochimica et Cosmochimica Acta., 27, 43–52.

Clayton R.N., O'Neil J.R., Mayeda T.K., 1972. Oxygen isotope exchange between quartz and water. Journal of Geophysical Research, 77(17), 3057–3067.

Coleman M., 1977. Sulphur isotopes in petrology: Journal of the Geological Society, 133, 593–608.

Cooke D.R., Simmons S.F., 2000, Characteristics and genesis of epithermal gold deposits: Reviews in Economic Geology, 13, 221–244.

Cromie P.W., 2010, Geological setting, geochemistry and genesis of the Sepon gold and copper deposits, Laos: Ph.D Thesis, v. University of Tasmania.

Giggenbach W.F., 1992. Isotopic shifts in waters from geothermal and volcanic systems along convergent plate boundaries and their origin. Earth and Planetary Science Letters, 113, 495–510.

Goldfarb R.J., 2023. Tempo and tectonic settings of orogenic gold deposits. Mineralium Deposita, 58, 1021–1047.

Goldfarb R.J., et al., 2015. Orogenic gold deposits: A proposed classification in a revised global metallogenic framework. Lithos, 233–234, 2–26.

Hedenquist J.W., Lowenstern J.B., 1994. The role of magmas in the formation of hydrothermal ore deposits. Nature, 370, 519–527.

Hodkiewicz P.F., Groves D.I., Davidson G.J., Weinberg R.F., Hagemann S.G., 2009. Influence of structural setting on sulphur isotopes in Archean orogenic gold deposits, Eastern Goldfields Province, Yilgarn, Western Australia. Mineralium Deposita, 44(2), 145–160.

Hoefs J., 2009. Stable Isotope Geochemistry (6th ed.). Springer, Berlin, 285p.

Hofstra A.H., Cline J.S., 2000, Characteristics and models for carlin-type gold deposits: Reviews in Economic Geology, 13, 163–220.

Hotson M.D., 2009, The geology and tectonic framework of Cu-Au prospects in the Phonsavan District, northern Laos, Unpublished Honours thesis, CODES University of Tasmania, Hobart, Australia, 115p.

Khin Zaw, Rodmanee T., Khositanont S., Thanasuthipitak T., Ruamkid S., 2007. Geology and genesis of Phu Thap Fah gold skarn deposit, northeastern Thailand: Implications for reduced gold skarn formation and mineral exploration; in Tantiwanit, W. (ed.). Proceedings of GEOTHAI'07 International Conference on Geology of Thailand, 21-22 November 2007, Bangkok, Thailand, 93–95.

Le T.X., Khin Zaw, Tran T.H., Luong Q.K., Du K.N., To B.X., 2025. Physico-chemical conditions and sources of Au mineralisation at Me Xi area, Central Truong Son Belt: Implication from fluid inclusion studies. Bulletin of the Geological Society of Malaysia.

Le T.X., Zaw K., To X.B., 2025a. Sources of Au-bearing mineralisation at the Me Xi Au deposit, Central Truong Son Belt, Vietnam: Evidence from sulfur isotopic composition. Journal of Mining and Earth Sciences, 66, 90–103.

Manaka T., 2008. Geological Setting and Mineralisation Characteristics of The Long Chieng Track and Ban Houayxai Deposit, Lao PDR: Master Thesis, University of Tasmania.

Matsumoto I., Kagi H., Nishido H., 2001. A new gas-extraction system for quantitative analysis of fluid inclusion gases using quadrupole mass spectrometry. Geochemical Journal, 35, 93–101.

Ngo X.D., Trinh H.S., Bui T.A., Nguyen T.T., Nguyen T.H.H., Nguyen D.T., Pham D.S., 2025. Physico-chemical conditions of Au mineralisation at the Xa Loi deposit, the Central Truong Son Belt, Vietnam: Insights from fluid inclusion studies. Vietnam Journal of Geology, A(380), 57–76.

Ngo Xuan Thanh, 2024. Study on establishing a genetic model and distribution patterns of selected prospective endogenous mineral deposits in the Kon Tum Massif. Specialized report of the national scientific research project, Code: ĐTĐL.CN.112/21. Ministry of Education and Training, Hanoi University of Mining and Geology.

Ngo Xuan T., Luong Quang K., Bui Vinh H., Tran

Thanh H., Nguyen Quoc H., Dinh Trong T., 2025. Petrogenesis and geological significance of the early Paleozoic S-Type granitic mylonite in the Southwestern Kon Tum Massif, Central Vietnam. Vietnam Journal of Earth Sciences, 47(3), 337–354. https://doi.org/10.15625/2615-9783/23115.

Nguyen H., Shinjo R., Tran T.H., Le D.L., Le D.A., 2021. Mantle geodynamics and source domain of the East Vietnam Sea opening-induced volcanism in Vietnam and neighboring regions. Vietnam Journal of Marine Science and Technology, 21(4), 393–417. https://doi.org/10.15625/1859-3097/16856.

Norman D.I., 1999. Methane and excess N_2 and Ar in geothermal fluid inclusion gases Evidence for organic matter contributions. Proceedings of the 24th Stanford Geothermal Workshop.

Ohmoto H., Rye R.O., 1979. Isotopes of sulfur and carbon. In: Barnes HL, editor. Geochemistry of Hydrothermal Ore Deposits. 2nd ed. New York. Wiley, 509–567.

Potter U., 2004. Nitrogen in crustal rocks: sources and behaviour during metamorphism and melting. Lithos, 73, 1–23.

Qiu H.N., Jiang Y.D., 2007. Sphalerite $^{40}Ar/^{39}Ar$ progressive crushing and stepwise heating techniques. Earth and Planetary Science Letters, 256(1–2), 224–232.

Qiu H.N., Wijbrans J.R., 2006. Paleozoic ages and excess ^{40}Ar in garnets from the Bixiling eclogite in Dabieshan, China: New insights from $^{40}Ar/^{39}Ar$ dating by stepwise crushing. Geochimica et Cosmochimica Acta, 71(24), 6046–6050.

Qiu H.N., Wu H.Y., Yun J.B., Brouwer F.M., Wijbrans J.R., 2011. High-precision $^{40}Ar/^{39}Ar$ age of the gas emplacement into the Songliao Basin. Geology, 39(5), 451–454.

Rollinson H.R., 1993, Using geochemical data: evaluation, presentation, interpretation, Longman Scientific & Technical Essex.

Sano Y., Marty B., 1995. Origin of nitrogen in the Earth's mantle. Chemical Geology, 119, 265–274.

Sasaki A., Ishihara S., 1979, Sulfur isotopic composition of the magnetite-series and ilmenite-series granitoids in Japan: Contributions to Mineralogy and Petrology, 68, 107–115.

Robert R., Seal II, 2006. Sulfur isotope geochemistry of sulfide minerals. Reviews in Mineralogy and Geochemistry, 61(1), 633–677.

Sheppard S.M.F., 1986. Characterization and isotopic variations in natural waters. In: Valley JW, Taylor HP Jr, O'Neil JR, editors. Stable Isotopes in High Temperature Geological Processes. Rev Mineralogy, 16, 165–183.

Taylor H.P. Jr., 1979. Oxygen and hydrogen isotope relationships in hydrothermal mineral deposits. In: Barnes HL, editor. Geochemistry of Hydrothermal Ore Deposits. 2nd ed. New York: Wiley, 236–277.

Thompson J.F.H., Newberry R.J., 2000. Gold deposits related to reduced granitic intrusions. In Hagemann S.G. & Brown P.E., Gold in 2000. Economic Geology, 13, 377–400.

Tran H.T., Zaw K., Halpin J.A., Manaka T., Meffre S., Lai C.K., Lee Y., Le H.V., Dinh S., 2014. The Tam Ky-Phuoc Son Shear Zone in central Vietnam: Tectonic and metallogenic implications. Gondwana Research, 26(1), 144–164.

Tran T.H., Tran T.A., Ngo T.P., Pham T.D., Tran V.A., Izokh A.E., Borisenko A.S., Lan C.Y, Chung S.L., Lo C.H., 2008. Permo-Triassic intermediate-felsic magmatism of the Truong Son belt, eastern margin of Indochina. Comptes Rendus Geoscience, 340(2–3), 112–126.

Tran Tuan A., Tran Trong H., Pham Ngoc C., Gregory Shellnutt J., Pham T.T., Izokh E.A., Soulintone O., 2022. Petrology of the Permian-Triassic granitoids in Northwest Vietnam and their relation to the amalgamation of the Indochina and Sino-Vietnam composite terranes. Vietnam Journal of Earth Sciences, 44(3), 343–368. https://doi.org/10.15625/2615-9783/17002.

Trinh Dinh H., Luu Cong T., Nguyen Tuan A., Tran Viet A., Phan Hoang G., Takahashi, Saadsy, 2021. Paleogene granite magmatism in the north of the Truong Son belt and implication for crustal evolution. Vietnam Journal of Earth Sciences, 43(4), 444–464. https://doi.org/10.15625/2615-9783/16444.

Watenphul A., Wunder B., Heinrich W., 2009. High-pressure ammonium-bearing silicates: Implications for nitrogen storage in the mantle. American Mineralogist, 94, 283–292.

Xiao M., et al., 2019. Gas release systematics of mineral-hosted fluid inclusions during stepwise crushing: Implications for $^{40}Ar/^{39}Ar$ geochronology of hydrothermal fluids. Geochimica et Cosmochimica Acta, 251(15), 36–55. https://doi.org/10.1016/j.gca.2019.02.016.

Table A1. QMS gas composition analysis

XL01						
Steps	Drops	CH$_4$	H$_2$O	N$_2$	Ar	CO$_2$
1	2	10,355	0,000	79,052	0,139	10,453
2	4	8,704	0,014	77,386	0,283	13,613
3	4	8,315	0,011	74,966	0,214	16,495
4	4	8,579	0,020	75,212	0,205	15,985
5	6	9,536	0,008	71,903	0,147	18,405
6	8	9,863	2,649	63,704	0,157	23,628
7	8	10,058	5,256	62,092	0,129	22,465
8	8	9,485	8,966	59,843	0,109	21,597
9	8	9,795	5,659	63,208	0,109	21,229
10	8	10,041	0,690	68,208	0,099	20,962
11	8	9,223	3,795	66,487	0,094	20,400
12	8	9,269	2,236	68,803	0,104	19,588
13	8	9,236	2,303	69,123	0,092	19,247
14	8	8,762	3,381	69,848	0,086	17,923
15	8	8,482	1,517	72,434	0,089	17,479
16	8	8,662	1,665	72,873	0,086	16,714
17	8	8,432	1,202	73,971	0,082	16,313
18	8	8,773	2,180	71,529	0,076	17,442
19	8	8,660	1,616	72,675	0,086	16,963
20	8	8,498	0,962	74,998	0,084	15,457
21	8	7,549	0,779	75,421	0,085	16,165
22	8	7,563	0,371	78,194	0,091	13,780
23	8	7,742	0,780	76,952	0,079	14,447
24	8	7,607	0,858	76,877	0,086	14,573
25	8	7,731	1,018	75,561	0,084	15,605
26	10	5,609	0,961	80,521	0,087	12,823
27	12	5,159	1,278	79,646	0,080	13,836
28	12	5,296	1,422	79,566	0,078	13,639
29	12	4,605	0,300	83,977	0,088	11,031
30	12	4,567	0,473	82,331	0,082	12,548
31	12	4,949	0,536	81,587	0,084	12,844
32	12	4,772	0,493	82,025	0,080	12,631
33	12	4,741	0,424	81,921	0,079	12,834
34	12	4,871	0,461	81,806	0,085	12,776
35	12	4,665	0,336	82,725	0,081	12,193
36	12	4,503	0,325	83,014	0,082	12,076
37	12	4,432	0,323	83,633	0,082	11,530
38	12	4,428	0,404	83,586	0,081	11,500
39	12	3,825	0,044	87,219	0,084	8,827
40	12	3,726	0,063	87,286	0,087	8,838
41	12	3,370	0,098	88,223	0,089	8,220
42	12	3,334	0,108	88,151	0,084	8,322
43	12	4,024	0,066	86,153	0,093	9,664
44	12	3,493	0,201	87,589	0,082	8,635
45	12	3,322	0,201	87,641	0,081	8,755
46	12	3,269	0,180	87,706	0,085	8,759
47	12	3,662	0,177	86,986	0,093	9,081
48	12	3,408	0,218	87,029	0,085	9,259
49	12	2,998	0,200	88,056	0,096	8,650
50	12	2,685	0,000	90,004	0,093	7,219
51	12	3,003	0,171	88,931	0,089	7,806

52	12	2,548	0,121	89,600	0,091	7,639
53	12	2,104	0,150	92,234	0,094	5,419
54	12	2,090	0,145	91,443	0,082	6,240
55	12	1,642	0,159	92,952	0,092	5,154
56	12	2,013	0,211	91,038	0,099	6,640
57	12	1,959	0,153	91,696	0,084	6,107
58	16	1,952	0,218	91,650	0,089	6,091
59	20	2,566	0,181	89,405	0,095	7,753
60	20	2,225	0,247	89,674	0,087	7,767
61	20	2,358	0,218	89,663	0,090	7,672
62	20	2,148	0,206	89,960	0,085	7,600
63	20	1,711	0,261	91,767	0,091	6,171
64	20	1,905	0,240	90,783	0,090	6,982
65	20	1,938	0,234	90,472	0,089	7,268
66	20	1,414	0,294	92,497	0,083	5,712
67	20	1,195	0,196	94,042	0,097	4,470
68	20	1,049	0,213	94,526	0,095	4,117
69	20	1,053	0,221	94,281	0,092	4,352
70	20	0,810	0,222	95,699	0,088	3,181
71	20	0,802	0,275	95,786	0,100	3,037
72	20	0,797	0,247	95,545	0,089	3,323
73	20	0,549	0,210	97,235	0,101	1,904
74	20	0,456	0,252	97,430	0,096	1,766
XL02						
Steps	**Drops**	**CH_4**	**H_2O**	**N_2**	**Ar**	**CO_2**
1	2	10,249	0,027	68,181	0,261	21,282
2	2	11,215	0,246	62,921	0,192	25,427
3	2	10,077	0,414	64,767	0,213	24,529
4	2	10,711	0,986	63,318	0,177	24,808
5	2	11,190	0,536	63,982	0,222	24,070
6	2	11,333	1,980	61,280	0,146	25,261
7	2	11,106	1,732	61,688	0,133	25,342
8	2	11,224	0,775	62,570	0,128	25,303
9	2	10,482	0,683	66,027	0,128	22,680
10	6	10,599	0,008	70,102	0,151	19,140
11	10	11,239	10,140	53,746	0,118	24,758
12	10	10,002	15,820	51,530	0,099	22,550
13	8	10,294	5,188	61,718	0,102	22,698
14	8	10,381	5,119	62,079	0,094	22,327
15	8	10,710	2,018	65,138	0,100	22,033
16	8	10,143	2,183	66,292	0,096	21,286
17	8	9,980	1,671	68,145	0,104	20,100
18	8	9,087	0,602	70,459	0,103	19,748
19	8	8,829	1,589	69,196	0,102	20,284
20	8	9,032	0,867	70,580	0,090	19,432
21	8	8,091	0,211	73,245	0,104	18,348
22	8	8,453	0,915	71,048	0,099	19,485
23	8	7,599	0,769	72,461	0,092	19,079
24	8	6,983	0,745	74,164	0,102	18,006
25	10	6,928	1,021	71,451	0,094	20,507
26	10	6,655	0,762	72,502	0,095	19,985
27	10	6,801	1,474	71,399	0,091	20,235
28	10	5,841	0,647	75,055	0,102	18,355
29	10	5,433	0,400	73,151	0,094	20,923

30	10	6,318	0,705	73,079	0,087	19,812
31	14	6,082	1,975	70,725	0,097	21,120
32	14	6,167	1,417	70,393	0,089	21,934
33	14	5,933	1,446	70,921	0,102	21,598
34	14	6,522	1,362	69,269	0,090	22,756
35	14	5,600	1,135	71,559	0,088	21,619
36	14	5,908	0,853	70,444	0,090	22,705
37	14	5,847	0,848	71,737	0,094	21,474
38	14	5,482	0,733	71,006	0,095	22,684
39	14	5,913	0,658	69,844	0,081	23,503
40	14	6,219	0,688	68,893	0,086	24,114
41	14	5,817	0,620	71,648	0,084	21,830
42	20	6,433	0,780	67,354	0,087	25,346
43	20	6,150	0,744	69,145	0,088	23,872
44	20	4,833	0,084	77,941	0,105	17,036
45	20	5,140	0,111	73,460	0,089	21,200
46	20	5,657	0,176	69,817	0,090	24,260
47	20	5,372	0,191	70,132	0,087	24,218
48	20	5,348	0,237	69,683	0,084	24,648
49	20	5,087	0,231	69,756	0,083	24,843
50	20	4,719	0,240	72,602	0,085	22,353
51	20	4,809	0,262	71,701	0,088	23,139
52	20	4,226	0,275	73,732	0,088	21,679
53	20	3,482	0,297	78,799	0,103	17,319
54	20	3,740	0,290	76,546	0,095	19,329
55	20	2,235	0,217	85,622	0,101	11,826
56	20	1,765	0,102	88,741	0,111	9,280
57	30	2,062	0,163	86,372	0,106	11,297
58	30	1,761	0,209	88,135	0,112	9,783
59	30	1,486	0,241	89,587	0,114	8,572
60	30	0,960	0,245	93,067	0,118	5,612
61	30	1,149	0,272	92,197	0,114	6,268
62	30	0,747	0,293	94,428	0,127	4,405